Nitrogen-Doped Holey Graphitic Carbon from 2D Covalent Organic Polymers for Oxygen Reduction

Zhonghua Xiang, Dapeng Cao,* Ling Huang, Jianglan Shui, Min Wang, and Liming Dai*

Since the seminal paper published by Geim et al., in 2004,[1] graphene has attracted tremendous interest due to its unique properties promising for various applications, including field-effect transistors,[2] metal-free electrocatalysts for oxygen reduction reaction (ORR) in fuel cells,[3] and electrodes in solar cells.[4] However, one of the major hurdles for application of graphene in electronics is the lack of band gap in its intrinsic form. Therefore, modulation of its electrical properties through band opening is of great technological importance.[1a,2,5] In this regard, N-doping has been widely studied as one of the most feasible methods to modulate the electronic and other properties of graphene and its derivatives.[6] N-doped graphene can be prepared either by in-situ doping during the graphene synthesis, for example via chemical vapor deposition,[3a,5b,7] or through post-treatment (i.e., post-doping) of pre-formed graphene nanostructures by physical exposure to nitrogen-containing moieties,[2,8] including N_2 plasma[9] and NH_3 annealing after N^+-ion irradiation.[10] Among the above-mentioned and many other reported N-doping methods to introduce nitrogen heteroatoms into graphene and its derivatives, none of the reported techniques allows for control of the exact locations of N atoms in the doped nanostructure. If realized, however, the location control of the N-dopant heteroatoms should provide us with powerful means to tailor the structure-property relationship for N-doped graphene (N-graphene) and other (carbon) nanomaterials.[9b,11] Recently, a series of covalent organic frameworks (COFs)[12] have been designed to form 'large' honeycomb graphene-like network with well-defined building blocks. Most recently, we have synthesized some covalent organic polymers (COPs)[12a,13] with precisely-controlled locations of N atoms and hole size (e.g., COP-2, COP-4, **Figure 1**) using triazine containing N-rich building blocks. In this work, we designed and synthesized more COP precursors (COP-T and COP-P, Figure 1) with different N distributions and hole sizes to produce a large class of COPs as N-containing molecular precursors with tunable N locations. Subsequent carbonization of these COPs led to well-controlled N-doped holey graphitic carbon materials with outstanding performance as electrocatalysts for oxygen reduction in fuel cells and electrode materials in high-performance supercapacitors. The observed electrocatalytic activities of these N-doped holey graphitic carbon materials can be correlated to the N locations in their COP molecular precursors, showing the technological power and importance of the N-location control for tailoring the structure and property of N-doped carbon nanomaterials.

Figure 1 shows the scheme for the synthesis of N-doped graphene analogues. As can be seen, we first synthesized COPs from triazine derivatives via Yamamoto polycondensation reaction.[13a,c] The resultant N-rich COPs were then subjected to carbonization in an inert atmosphere to produce the N-doped graphitic carbon materials, which we named as COP graphene for simplicity. Four COP graphene derivatives with different N-containing building blocks of varied N doping levels and porous structures were obtained (Figures 1a–1d). The exact positions of the N-dopant heteroatoms in the resultant COP graphene derivatives depend strongly on the detailed chemical structure and exact N positions in the building blocks of the respective COP precursor, which can be precisely controlled. Therefore, it is possible to tune the position of N atoms in the COP graphitic materials by using tailor-made N-containing building blocks for controlled synthesis of the COP precursors. In this study, structurally well-defined and hydrothermally stable COP precursors (COP-2, COP-4, COP-P and COP-T) were synthesized from N-containing monomers with different structures by the Ni-catalyzed Yamamoto reaction[13a,c] (Figure 1). Since the structural characterization of COP-2 and COP-4 macromolecules has been reported in our previous publication,[13a] we will focus on the molecular structure characterization of the newly-synthesized COP-T and COP-P in the present study. The absence of C-Br stretching peak around 512 cm^{-1} in the FT-IR spectra of COP-P and COP-T (Figures S1 and S2) indicates the occurrence of the efficient phenyl-phenyl coupling in Yamamoto reaction for a complete Br elimination. Moreover, the ^{13}C/MAS spectra of COP-P and COP-T indicate the existence of main structures of the monomers of TBBPP and TBYT, respectively (**Figure 2**a and Figure S3a). Of particular interest, the SEM image of COP-P shows a beautiful flower-like structure consisting of thin "petals" (Figures 2b and 2c). The TEM images given in Figures 2d and 2e further revealed the layered texture of COP-P.

We further performed carbonization to convert the resultant N-rich COPs to N-doped COP graphitic carbon materials. The optimized carbonization temperature for COP-4 was found to

Dr. Z. Xiang, Prof. Dr. D. P. Cao, L. Huang
State Key Lab of Organic-Inorganic Composites
Beijing University of Chemical Technology
Beijing 100029, P.R. China
E-mail: caodp@mail.buct.edu.cn
Dr. J. L. Shui, M. Wang, Prof. L. M. Dai
Center of Advanced Science and Engineering
for Carbon (Case4Carbon)
Department of Macromolecular Science
and Engineering
Case Western Reserve University
10900 Euclid Avenue
Cleveland, OH, 44106, USA
E-mail: liming.dai@case.edu

**ADVANCED
MATERIALS**
www.advmat.de

Materials
Views
www.MaterialsViews.com

COMMUNICATION
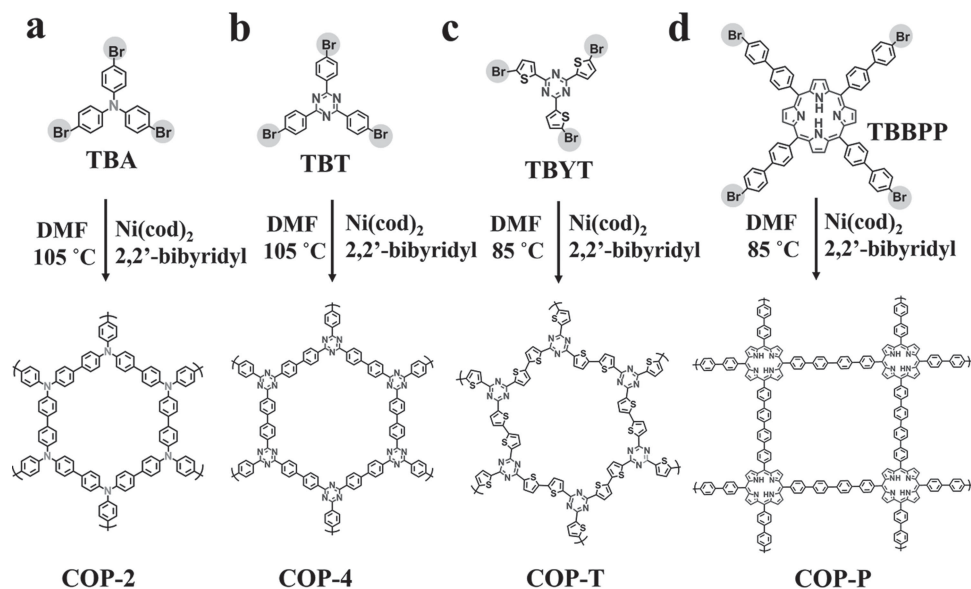
Figure 1. Schematic diagram of synthesis of N-rich COP precursors. (a–d), Schematic representation of synthesis of COP-2, COP-4, COP-T and COP-P through monomers tris(4-bromophenyl)amine (TBA), 2,4,6-tris-(4-bromo-phenyl)-[1,3,5] triazine (TBT), (4′-bromo-biphenyl-4-yl)- porphyrine (TBBPP) and 2,4,6-tris (5-bromothiophen-2-yl)-1,3,5-triazine (TBYT), respectively, using nickel- catalyzed Yamamoto-type Ullmann cross-coupling reaction. The actual structures of these statistical COPs will be more complex than those represented here.

be 950 °C, as confirmed by the following ORR activity (vide infra; Figure S19) as well as the supercapacitor performance (see the Supporting Information). For simplicity, we marked these COP graphitic carbon samples as C-COP-X-Temp (X = 2, 4, P and T; Temp refers to the carbonization temperature and is omitted when Temp = 950 °C).

As can be seen in **Figure 3**a, C-COP-4 possesses a slightly stronger G band than the corresponding D band in its Raman spectrum. Especially, the sharp 2D band in C-COP-4 suggests existence of few-layer graphene-like structures, also confirmed

by the SEM (Figure 3e) and atomic force microscopy (AFM) images (Figure 3k). Other three COP graphitc samples also exhibit a stronger G band than the corresponding D band in the respective Raman spectra (Figure S6). The observed relatively high intensity of D band for all the four COP graphitic samples with respect to that of CVD-grown graphene[5b] is attributable to the long range disorder associated with those interdispersed small holes of rich edge defects (vide infra). The introduction of N-dopant heteroatoms into the COP graphitic networks contributes also to the D band intensity. SEM images of C-COP-4
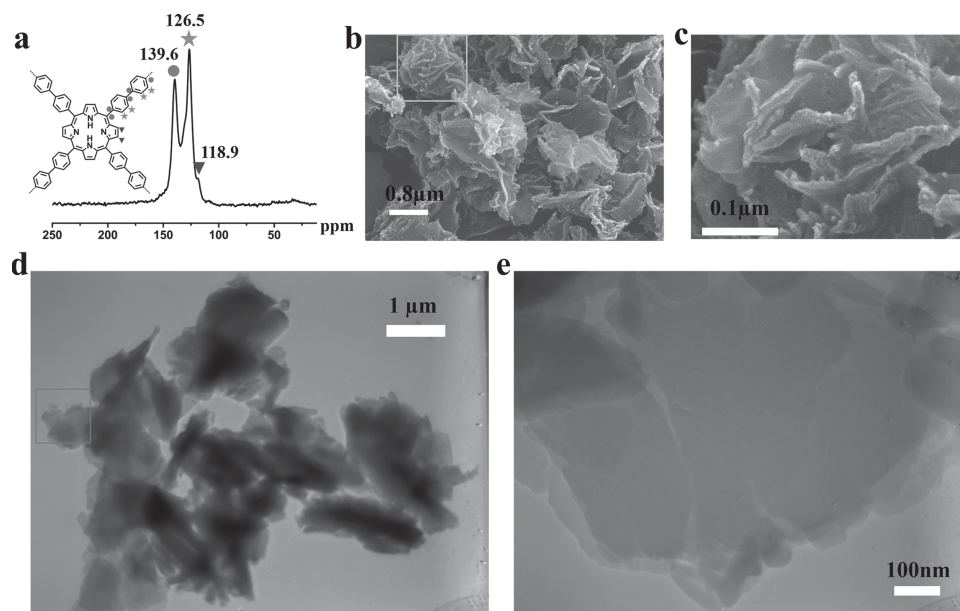
Figure 2. Structural characterization and morphology of COP-P. (a) ^{13}C CP/MAS spectra of COP-P and its peak assignments. (b) SEM image. (c) is the enlargement of the boxed area in (b). (d) TEM image. (e) is the enlargement of the boxed area in (d).
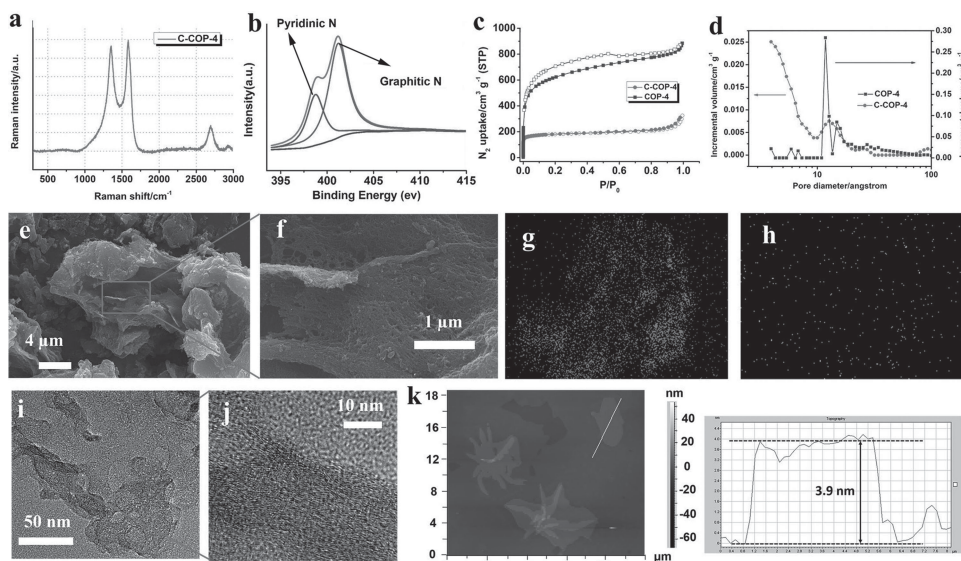
Figure 3. Characterization of N-doped COP graphitic carbon (C-COP-4). (a) Raman spectra. (b) High-resolution XPS N 1s spectrum of C-COP-4. The N 1s peak can be split to two Lorentzian peaks at 398.7 and 401.3 eV, which are indicated by arrows. (c) N_2 adsorption isotherms of C-COP-4 at 77 K. Solid and open symbols represent adsorption and desorption, respectively. (d) NLDFT pore size distributions of COP-4 and C-COP-4 by incremental pore volume. (e), (f), SEM images. (g),(h), SEM mapping photograph of C atoms (g) and N atoms (h) in the box of h. (i),(j), TEM images. (k) Tapping-mode AFM images and the corresponding height analyses along the lines marked in the AFM image.

given in Figures 3e and 3f show curled layers with holes while C-COP-P exhibits a "petal" shaped morphology (Figure S7). The corresponding SEM elemental mapping reveals that both carbon (red) and nitrogen (green) atoms distribute homogeneously within the C-COP-4 and C-COP-P (Figures 3g and 3h and Figures S7c and S7d, respectively). Also, the corresponding TEM images show the multilayered graphene-like texture with a graphitic lattice fringe (Figure 3i-3j and Figures S7 and S8). Unlike their COP precursors, XRD spectra for most of the carbonized C-COPs showed a pronounced (0 0 2) graphitic peak at 26° (Figures S10-S12), suggesting the formation of graphitic structures during carbonization. The weight percentage content of N in all the four C-COP samples remained still high (e.g., 5.29 wt% for C-COP-T, Table S1), though it is lower than that of the corresponding COP precursors because the high-temperature carbonization could have caused the inevitable loss of N atoms. XPS results show that the atomic percentages of N in C-COP-2, C-COP-4, C-COP-P and C-COP-T were found to be about 2.43, 3.31, 2.68 and 4.14 wt%, which is consistent with those from the elemental analyses done on a Thermo Fisher Scientific Elemental Analyzer (2.79, 3.81, 2.81 and 5.28 wt%; Table S1 and S2). The XPS N 1s spectra of C-COP-2, C-COP-4 and C-COP-T (Figure 3b and Figures S13–16) could be deconvoluted into two sub-peaks: "graphitic" N at ~401.3 eV and "pyridinic" N at ~398.7 eV. The "pyridinic" N species in these C-COP samples suggest the existence of some skeletons of COP precursor and the "graphitic" N component is, most probably, arising from the formation of graphitic structures during carbonization. As expected, therefore, C-COP-P graphitic carbon shows a dominant "pyrrolic" peak at 400.1 eV (Figure S15) corresponding to the intrinsic "pyrrolic" N in the COP-P precursor. The main sharp peak at ~284.8 eV in the C 1s spectra for all the four COP graphitic samples (Figures S13-S16)

corresponds to the graphitic sp^2-C, indicating most of the C atoms in the C-COP graphitic carbon materials are arranged in the intrinsic conjugated form as in the COP precursors. Apart from the graphitic sp^2-C component, the C 1s spectra for all the four C-COP samples contain also sp^2-C-N, sp^3-C-N, sp^3-C, and/or C-S (C-COP-T), but without O-bonded C component (Figures S13-S16). Therefore, the physically adsorbed oxygen or water molecules are responsible for the O 1s peaks seen in Figures S13-S16.[3a,5b] Interestingly, the N_2 isotherms at 77 K show the porous nature of these COP graphitic samples (Figures 3c and 3d and Table S3). Although the porosity of COP-4 (2015 m^2 g^{-1}) reduced dramatically after carbonization (569 m^2 g^{-1}), the predominant pores in the C-COP-4 graphitic carbon have a hole size of ~11.8 Å similar to those in the COP-4 precursor, suggesting again the existence of skeleton of COP-4 precursor even after carbonization.

Based on the above results, it is valid to predict the electronic properties using the skeleton of the COP precursors as model structures for density function theory (DFT) calculations. By calculating the partial charge density, we found that electrons are mainly provided by the N heteroatoms in all the four samples due to the stronger electronegativity of N than that of C atoms (**Figure 4**). Compared to the amine groups in C-COP-2, the planar π-electron system associated with triazine groups leads to a better charge mobility for C-COP-4. Electrons within the phenyl groups of C-COP-P (Figure 4d) apparently display a lower degree of freedom than those in C-COP-2 (Figure 4a) and C-COP-4 (Figure 4b). Therefore, the electrons in C-COP-P show a lower mobility than those in C-COP-2 and C-COP-4. Compared to two phenyl groups in C-COP-2 and C-COP-4, the four phenyl groups between two porphyrin rings in C-COP-P provide a much longer electronic transmission channel. Therefore, C-COP-P displays a lower electronic activity than
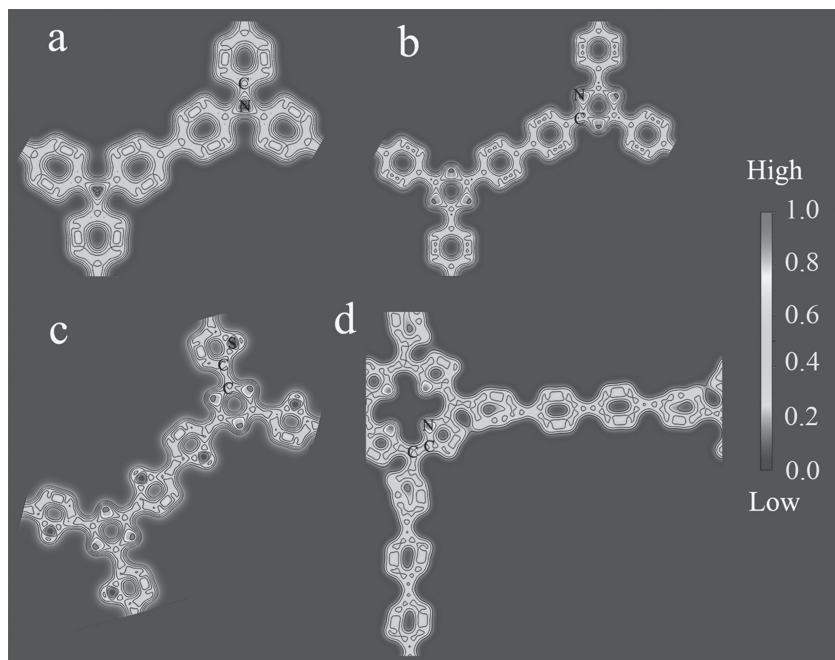
Figure 4. Partial charge density of N-doped COP graphene. (a) C-COP-2. (b) C-COP-4. (c) C-COP-T. (d) C-COP-P. The values of contours in the plots are form 0.001 e Bohr^{-3} to 1.000 e Bohr^{-3} with an increment of 0.903 e Bohr^{-3}.

Oxygen reduction plays an important role in regulating the performance of a fuel cell. However, the development of ORR electrocatalysts with high activity at low cost still remains a great challenge.[14] Recent studies have demonstrated the potential to use metal-free electrocatalysts[3a,6a,14b,15] to replace Pt-based electrodes in fuel cells. In this work, we investigated electrocatalytic activities of the COP graphene for ORR in 0.1 M KOH aqueous solution by using various electrochemical analytic tools, including cyclic voltammetry (CV), rotating disk electrode (RDE), rotating ring disk electrode (RRDE), and chronoamperometric measurements. As shown in **Figure 5**a, all the four C-COP samples show well-defined cathodic ORR peaks in aqueous solution of KOH (0.1 M) saturated with O_2, but not N_2, within the potential range from 0 to 1.0 V. As expected, C-COP-4 shows a ORR peak at the most positive potential (Figure 5a, 0.79 V relative to the reversible hydrogen electrode, RHE) among all the COP graphitic electrodes, though it is not as good as the commercial Pt/C electrode (C2–20, 20% platinum on Vulcan XC-72R; E-TEK). The electrocatalytic activities are

C-COP-2 or C-COP-4. It is also noted that the charge density of S atoms in C-COP-T (Figure 4c) is very low so that the electron transport slows down over the thiophene S atoms, and hence C-COP-T becomes semiconducting. Above analysis indicates that C-COP-4 should display the best electronic properties among the four C-COP graphitic carbon samples studied here. The charge redistribution caused by N-doping could make the C-COP graphitic carbon materials good candidates as efficient metal-free electrocatalysts for oxygen reduction.[6e] Actually, the DFT calculations support the following experimental studies on the ORR of the C-COP graphitic carbon materials.

in the order of C-COP-4 > C-COP-2 > C-COP-T > C-COP-P (Figure 5 and Figure S24), as predicated by the DFT calculations (vide supra). Compared to C-COP-P, the more positive ORR peak potential (Figure 5a) and slightly higher diffusion current density (Figure 5b) for C-COP-T could be attributed to its slightly higher graphitization degree (Figure S6). Overall, the ORR performance of the C-COP graphitic carbon materials correlated well to the calculated electronic properties for the COP precursors with well-defined N locations and hole sizes.

To further investigate the ORR performance, we carried out the linear sweep voltammetric (LSV) measurements on a rotating
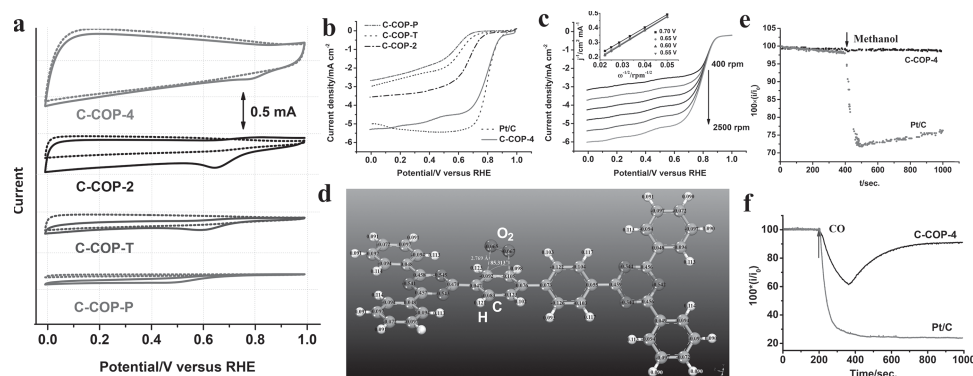
Figure 5. Electrochemical characterization of COP graphene ORR catalysts. (a) CV curves of COP graphitic electrodes in O_2-saturated 0.1 M KOH at a sweep rate of 50 mV s^{-1}. (b) LSV curves of COP graphitic electrodes in O_2-saturated 0.1 M KOH at 1600 rpm at a sweep rate of 5 mV s^{-1}. (c) RDE curves of C-COP-4 in O_2-saturated 0.1 M KOH with different speeds at a scan rate of 5 mV s^{-1} (the inset showing the Koutecky-Levich plots of the C-COP-4 derived from RDE measurements). (d) Calculated charge distributions for the cluster for optimal O_2 adsorbed on the COP-4 graphitic carbon. The measured distance is presented in angstroms, and the measured angle is presented in degrees. (e and f) Methanol and CO-poison effect evaluation on i-t chronoamperometric responses, respectively, for ORR at Pt/C (light gray) and C-COP-4 (black) electrodes. The arrow indicates the addition of 3 mL methanol into the O_2-saturated electrochemical cell after about 400 s in (e) and the addition of 55 mL min^{-1} CO gas into the 550 mL min^{-1} O_2 flow saturated electrochemical cell in (f).

disk electrode (RDE) for four COP graphitic samples (Figure 5b). As predicted in the DFT calculations, C-COP-4 shows the best ORR activity among the four samples. It can be seen in Figure 5b that the LSV curve of the C-COP-4 shows a one-step process, as the case of the Pt/C catalyst (Figure S23). C-COP-4 exhibits the similar onset potential as the Pt/C catalyst, and the half-wave potential of the C-COP-4 electrode reaches 0.78 V, which is also very close to 0.80 V of Pt/C. The transferred electron number (n) per O_2 molecule for C-COP-4 calculated by Koutecky-Levich (K-L) equation is 3.90 at 0.55~0.70 V (Figure 5c), which is similar to 3.88 calculated by the RRDE curves (Figure S24).[12]

To better understand the O_2 reduction mechanism on the C-COP-4 graphitic carbon, we further carried out the first principles calculations. Our calculations indicate that O_2 molecules prefer to be adsorbed on the top of the phenyl group adjacent to triazine groups via Yeager model[16] on the C-COP-4 graphitic carbon (Figure 5d and Figures S27-S31). Since the N atom in the trizaine group possesses a strong electron affinity with a substantially high negative charge density to counterbalance C atoms, the O atoms with a negative charge density in the adsorbed O_2 molecules prefer to stay around the C atoms in phenyl groups with a relatively lower positive charge density rather than those C atoms adjacent to N atoms. Moreover, the bond length of O_2 molecules adsorbed on the C-COP-4 graphitic carbon is elongated from 1.216 Å in pure O_2 molecules to 1.232 Å at γ site (Table S4), suggesting that the parallel diatomic adsorption could effectively weaken the O-O bonding to facilitate ORR at the C-COP-4 electrode. Therefore, the N-doped C-COP-4 electrode can efficiently create the metal-free active sites for electrochemical reduction of O_2 through the charge redistribution.[6e] The C-COP-4 electrode was further demonstrated to be free from the methanol crossover effect (Figure 5e). Although the C-COP-4 electrode showed a weak CO-poisoning effect, possibly due to the hole (edge) adsorption, its electrocatalytic activity can be self-recovered to 90% within a short period of time (~5 minutes) (Figure 5f). Furthermore, the C-COP-4 electrode exhibited a remarkably better long-term stability than the commercial Pt/C catalyst (Figure S25). These results clearly indicate that the C-COP-4 graphitic carbon is a promising metal-free ORR catalyst for fuel cells. Apart from the demonstrated high electrocatalytic activities towards ORR, our preliminary results indicate that these N-doped holey C-COPs are also desirable electrode materials in supercapacitors for efficient charge storage (see Figure S32 and associated discussions in the Supporting Information for details).

In summary, we have developed a class of new covalent organic polymers (COPs) with precisely-controlled locations of N atoms and hole sizes, from which well-controlled N-doped holey graphitic carbon materials were obtained by post-synthesis carbonization. The newly-developed N-doped holey graphitic carbon materials were demonstrated to be promising for efficient energy conversion and storage, particularly as efficient metal-free electrocatalysts for oxygen reduction reaction (ORR) in fuel cells. Our experimental efforts were complemented by the first principles calculations. The combined experimental and theoretical approach showed that the structure and property of the COP precursors could be translated into the resultant graphitic carbon materials, providing a new strategy to location control of N-dopant heteroatoms in the N-doped graphitic structure, which otherwise is impossible to achieve with conventional N-doping techniques. Furthermore, the methodology developed in this work should be applicable to graphitic carbon materials, including graphene and its derivatives, doped by other heteroatom(s) (e.g., B, S, P) with controlled locations of the dopant heteroatoms, and hence well-defined properties. Therefore, this work has opened up new possibilities for the development of a large variety of heteroatom-doped carbon nanomaterials with well-controlled structures and properties attractive for multifunctional applications, including new materials for energy conversion and storage, thermal management, electronics, and sensors.

Supporting Information

Supporting Information is available from the Wiley Online Library or from the author.

Acknowledgements

[1] a) K. S. Novoselov, A. K. Geim, S. V. Morozov, D. Jiang, Y. Zhang, S. V. Dubonos, I. V. Grigorieva, A. A. Firsov, *Science* **2004**, *306*, 666–669; b) A. K. Geim, K. S. Novoselov, *Nat. Mater.* **2007**, *6*, 183–191.

[2] X. R. Wang, X. L. Li, L. Zhang, Y. Yoon, P. K. Weber, H. L. Wang, J. Guo, H. J. Dai, *Science* **2009**, *324*, 768–771.

[3] a) L. Qu, Y. Liu, J.-B. Baek, L. Dai, *ACS Nano* **2010**, *4*, 1321–1326; b) K. Parvez, S. Yang, Y. Hernandez, A. Winter, A. Turchanin, X. Feng, K. Müllen, *ACS Nano* **2012**, *6*, 9541–9550.

[4] a) Y. Xue, J. Liu, H. Chen, R. Wang, D. Li, J. Qu, L. Dai, *Angew. Chem. Int. Ed.* **2012**, *51*, 12124–12127; b) S. Osella, A. Narita, M. G. Schwab, Y. Hernandez, X. Feng, K. Müllen, D. Beljonne, *ACS Nano* **2012**, *6*, 5539–5548.

[5] a) C. Berger, Z. Song, X. Li, X. Wu, N. Brown, C. Naud, D. Mayou, T. Li, J. Hass, A. N. Marchenkov, E. H. Conrad, P. N. First, W. A. de Heer, *Science* **2006**, *312*, 1191–1196; b) D. Wei, Y. Liu, Y. Wang, H. Zhang, L. Huang, G. Yu, *Nano Lett.* **2009**, *9*, 1752–1758.

[6] a) L. Dai, D. W. Chang, J.-B. Baek, W. Lu, *Small* **2012**, *8*, 1130–1166; b) J. Zhang, F. Zhao, Z. Zhang, N. Chen, L. Qu, *Nanoscale* **2013**, *5*, 3112–3126; c) L. Dai, *Acc. Chem. Res.* **2012**, *46*, 31–42; d) D. Yu, L. Dai, *J. Phys. Chem. Lett.* **2009**, *1*, 467–470; e) K. P. Gong, F. Du, Z. H. Xia, M. Durstock, L. M. Dai, *Science* **2009**, *323*, 760–764; f) L. Zhao, R. He, K. T. Rim, T. Schiros, K. S. Kim, H. Zhou, C. Gutiérrez, S. P. Chockalingam, C. J. Arguello, L. Pálová, D. Nordlund, M. S. Hybertsen, D. R. Reichman, T. F. Heinz, P. Kim, A. Pinczuk, G. W. Flynn, A. N. Pasupathy, *Science* **2011**, *333*, 999–1003; g) D. Yu, K. Goh, L. Wei, H. Wang, Q. Zhang, W. Jiang, R. Si, Y. Chen, *J. Mater. Chem. A* **2013**, *1*, 11061–11069; h) D. Yu, L. Wei, W. Jiang, H. Wang, B. Sun, Q. Zhang, K. Goh, R. Si, Y. Chen, *Nanoscale* **2013**, *5*, 3457–3464.

[7] Y. Li, Y. Zhao, H. Cheng, Y. Hu, G. Shi, L. Dai, L. Qu, *J. Am. Chem. Soc.* **2011**, *134*, 15–18.

[8] S. Yang, R. E. Bachman, X. Feng, K. Müllen, *Acc. Chem. Res.* **2012**, *46*, 116–128.

[9] a) Y. Wang, Y. Shao, D. W. Matson, J. Li, Y. Lin, *ACS Nano* **2010**, *4*, 1790–1798; b) H. M. Jeong, J. W. Lee, W. H. Shin, Y. J. Choi, H. J. Shin, J. K. Kang, J. W. Choi, *Nano Lett.* **2011**, *11*, 2472–2477.

[10] B. D. Guo, Q. A. Liu, E. D. Chen, H. W. Zhu, L. A. Fang, J. R. Gong, *Nano Lett.* **2010**, *10*, 4975–4980.

[11] Z. Xu, in *In Physics and Applications of Graphene – Experiments*, (Ed.: S. Mikhailov), InTech: Rijeka, Croatia, **2011**.

[12] a) Z. H. Xiang, D. P. Cao, *J. Mater. Chem. A* **2013**, *1*, 2691–2718; b) F. Schlütter, F. Rossel, M. Kivala, V. Enkelmann, J.-P. Gisselbrecht, P. Ruffieux, R. Fasel, K. Müllen, *J. Am. Chem. Soc.* **2013**, *135*, 4550–4557; c) J. W. Colson, W. R. Dichtel, *Nat. Chem.* **2013**, *5*, 453–465; d) J. W. Colson, A. R. Woll, A. Mukherjee, M. P. Levendorf, E. L. Spitler, V. B. Shields, M. G. Spencer, J. Park, W. R. Dichtel, *Science* **2011**, *332*, 228–231; e) X. Feng, X. Ding, D. Jiang, *Chem. Soc. Rev.* **2012**, *41*, 6010–6022; f) R. Dawson,

A. I. Cooper, D. J. Adams, *Prog. Polym. Sci.* **2012**, *37*, 530–563; g) M. Bieri, M. Treier, J. Cai, K. Ait-Mansour, P. Ruffieux, O. Groning, P. Groning, M. Kastler, R. Rieger, X. Feng, K. Mullen, R. Fasel, *Chem. Commun.* **2009**, 6919–6921.

[13] a) Z. H. Xiang, D. P. Cao, *Macromol. Rapid Commun.* **2012**, *33*, 1184–1190; b) Z. H. Xiang, X. Zhou, C. H. Zhou, S. Zhong, X. He, C. P. Qin, D. P. Cao, *J. Mater. Chem.* **2012**, *22*, 22663–22669; c) Z. H. Xiang, D. P. Cao, W. C. Wang, W. T. Yang, B. Y. Han, J. M. Lu, *J. Phys. Chem. C* **2012**, *116*, 5974–5980.

[14] a) Y. Y. Liang, Y. G. Li, H. L. Wang, J. G. Zhou, J. Wang, T. Regier, H. J. Dai, *Nat. Mater.* **2011**, *10*, 780–786; b) L. Qu, L. Dai, M. Stone, Z. Xia, Z. L. Wang, *Science* **2008**, *322*, 238–242.

[15] a) L. Y. Feng, Y. Y. Yan, Y. G. Chen, L. J. Wang, *Energ Environ. Sci.* **2011**, *4*, 1892–1899; b) S. Y. Wang, D. S. Yu, L. M. Dai, *J. Am. Chem. Soc.* **2011**, *133*, 5182–5185; c) S. Y. Wang, D. S. Yu, L. M. Dai, D. W. Chang, J. B. Baek, *ACS Nano* **2011**, *5*, 6202–6209; d) Y. Zheng, Y. Jiao, J. Chen, J. Liu, J. Liang, A. Du, W. M. Zhang, Z. H. Zhu, S. C. Smith, M. Jaroniec, G. Q. Lu, S. Z. Qiao, *J. Am. Chem. Soc.* **2011**, *133*, 20116–20119.

[16] Z. Shi, J. J. Zhang, Z. S. Liu, H. J. Wang, D. P. Wilkinson, *Electrochim. Acta* **2006**, *51*, 1905–1916.